Tuning the Deoxygenation of Bulk-Dissolved Oxygen in Copper

Chaoran Li,[†] Peihong Zhang,[‡] Jianyu Wang,[†] Jorge Anibal Boscoboinik,[§] and Guangwen Zhou*,[†]

[†]Department of Mechanical Engineering and Materials Science and Engineering Program, State University of New York at Binghamton, New York 13902, United States

[‡]Department of Physics, University at Buffalo, State University of New York, Buffalo, New York 14260, United States

[§]Center for Functional Nanomaterials, Brookhaven National Laboratory, Upton, New York 11973, United States

S *Supporting Information*

ABSTRACT: Using synchrotron-based ambient-pressure X-ray photoelectron spectroscopy, we report the tuning of the deoxygenation process of bulk dissolved oxygen in copper via a combination of H_2 gas flow and elevated temperature. We show that a critical temperature of ∼580 °C exists for driving segregation of bulk dissolved oxygen to form chemisorbed oxygen on the Cu surface, which subsequently reacts with hydrogen to form OH species and then H_2O molecules that desorb from the surface. This deoxygenation process is tunable by a progressive stepwise increase of temperature that results in surface segregation of oxygen from deeper regions of bulk Cu. Using atomistic simulations, we show that the bulk-dissolved oxygen occupies octahedral sites of the Cu lattice and the deoxygenation process involves oxygen migration between octahedral and tetrahedral sites with a diffusion barrier of ∼0.5 eV.
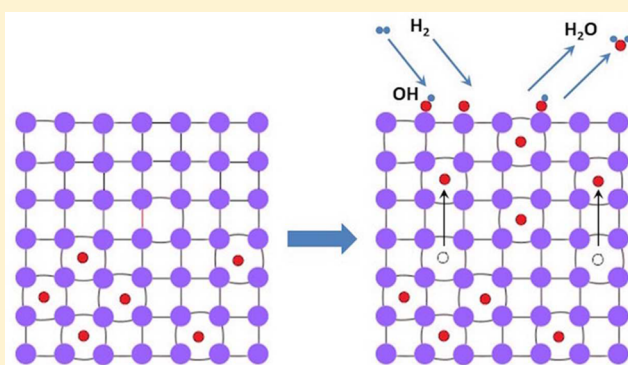
1. INTRODUCTION

Interstitial solid solutions result when the size difference between atoms is sufficiently large such that the smaller atoms can fit into interstices in the crystal lattice of the larger atoms. Such solutions occur, for example, when relatively small atoms such as those of hydrogen, oxygen, nitrogen or carbon dissolve in a metal lattice. The presence of interstitial elements in appreciable quantities can often lead to drastic changes in properties, that is, corrosion resistance and catalytic function at surface and subsurface regions,[1−3] fracture strength at grain boundaries,[4,5] plastic deformation at dislocations,[6,7] and adhesion and integrity at heterophase interfaces.[8] Therefore, the effects of interstitial impurities in metals can easily manifest themselves by causing various macroscopic phenomena.

The incorporation of desired impurities (or dopants) into the bulk has been studied extensively to modify or achieve desired bulk properties.[9−11] In contrast, the fundamental understanding on the reversed process, that is, removal of impurities, is very limited. Macroscopically speaking, the removal of impurities from a material is usually time-consuming, energy intensive, and very costly. The reason is of thermodynamic nature, that is, removing impurities means reducing the entropy of the system and this would require a large amount of energy as predicted by the second law of thermodynamics. Microscopically, the removal of impurities from the bulk has to involve mass transport from the bulk to the subsurface region and then to the surface, but detailed information about the true nature of such surface and subsurface processes is rather poor. The reason why such

processes are poorly investigated is that very few surface science techniques exist, which can be applied to the investigation of the dynamic changes in the surface and subsurface region. It is also difficult to distinguish between surface and subsurface states. Recent advances in instrumentation have made it possible to investigate the surface and subsurface region exposed to high gas pressures with ambient-pressure X-ray photoelectron spectroscopy (AP-XPS).[1,12−15] Synchrotron-based AP-XPS provides a unique window for probing the atomic processes of the segregation of impurities from the bulk under a more practical condition, namely, the near-ambient oxygen pressure that may result in bulk-dissolved oxygen and thereafter the near-ambient hydrogen pressure that leads to the deoxygenation of the bulk-dissolved oxygen.

The rich interaction between oxygen and Cu makes Cu one of the best catalytic materials for industrial reactions including methanol oxidation,[16−19] the water−gas shift reaction,[20−22] controllable synthesis of low-dimensional materials,[23−25] and CO_2 reduction.[26] For instance, Cu is by far the most widely used catalytic substrate to grow graphene because of its low cost but high catalytic activity. Oxygen impurities are present in different concentrations in commercially available Cu and the surface segregation of oxygen out of Cu bulk can significantly influence the growth behavior of graphene domains on the Cu substrate by modifying the adsorption, dissociation, and surface

diffusion of hydrocarbons.[27−29] The behavior of oxidation of copper and reduction of copper oxides has thus received considerable attention.[30−37] Oxygen surface segregation (or oxygen exposure) provides a convenient tuning parameter for modifying the surface reactivity and selectivity of Cu.[38,39] A fundamental understanding of the deoxygenation of bulk dissolved oxygen in metals, particularly Cu, is therefore technologically important and needs to be elucidated. In this work, we demonstrate, with a combination of the AP-XPS experiments and density-functional theory (DFT) modeling, the removability of bulk-dissolved oxygen in Cu, in particular, how the deoxygenated process can be manipulated via temperature and hydrogen gas.

2. EXPERIMENTAL AND COMPUTATIONAL METHODS

AP-XPS experiments were performed at CFN AP-PES endstation at the CSX-2 beamline of the National Synchrotron Light Source II (NSLS-II), Brookhaven National Laboratory. The AP-XPS station is equipped with a main chamber with the base pressure lower than 5×10^{-9} Torr, a SPECS Phoibos NAP 150 hemispherical analyzer, and an Ar-ion sputtering gun. The AP-XPS system has several differential pumping stages between the reaction chamber and the hemispherical analyzer which allows keeping ultrahigh vacuum (UHV) conditions (lower than 1×10^{-7} Torr) in the analyzer when the pressure in the analysis chamber is a few Torr. Photoemitted electrons leave the high-pressure chamber through a small aperture in a conical piece into the differentially pumped transfer lenses system toward the electron energy analyzer. XPS spectra can be acquired in this system at pressures of up to ∼5 Torr. The photon energy range of the beamline is from 250 to 2000 eV, which covers the O 1s, C 1s, and Cu 2p core levels relevant for the current work. Spectra of O 1s, Cu 2p, and Cu $L_3M_{45}M_{45}$ were acquired in situ in the presence of gas.

The Cu(110) single crystal (Princeton Scientific Corp, purity = 99.9999%) is a top-hat shaped disc (1 mm thick and 8 mm in diameter), cut to within 0.1° to the (110) crystallographic orientation and polished to a mirror finish. The sample was heated via a ceramic button heater, and its temperature was monitored with a type-K thermocouple. The crystal was cleaned by repeated cycles of Ar$^+$ bombardment (5×10^{-5} Torr of Ar gas, 1 μA cm^{-2}, 1.0 keV, 20 min) at room temperature, followed by annealing at 600 °C (UHV, 10 min) until no O and C spectra could be detected by XPS (see Figure S1 in the Supporting Information). Oxygen gas (purity = 99.9999%) was directly introduced to the system through a variable-pressure leak valve to oxidize the freshly cleaned Cu(110) surface for 1 h at 350 °C and 1 Torr of O$_2$ gas, which resulted in the formation of a Cu oxide layer on the surface in addition to a sufficient amount of oxygen impurity in the Cu bulk. Reduction of the oxidized Cu surface and the subsequent removal of O impurity in the bulk were performed by flowing 0.2 Torr of H$_2$ gas at different temperatures. Unless specified otherwise, the photon energy chosen for the collection of XPS spectra is 1150 eV in order to gain access to Cu 2p levels (953 and 932 eV) and avoid overlapping with Auger emissions. Identification of the different chemical states of oxygen on the surface and in the near subsurface region was performed using depth profiling by variation of the incident photon energy from 650 to 1250 eV. All spectra were collected at the takeoff angle of 20° and binding energies in each spectrum were referred to the Fermi level, analyzed with a Gaussian/Lorentz product formula and Voigt lines using a Shirley-type background. Linear-type

background was used for peak deconvolution and fitting. The O 1s, Cu 2p, and Cu $L_3M_{45}M_{45}$ were monitored to investigate changes in spectral features and binding energies during the oxide reduction. Binding energies and full width at half-maximum (fwhm) values of the component peaks are compiled in Table S1 in the Supporting Information.

The density-functional theory (DFT) calculations were performed using Vienna ab initio simulation package (VASP)[40−43] with the generalized gradient approximation (GGA) of Perdew−Wang (PW91)[44] for the exchange-correlation functional and projector augmented wave (PAW)[45,46] potentials in conjunction with a planewave cutoff energy of 380 eV. The calculations were carried out with broadening of the Fermi surface according to the Methfessel−Paxton smearing technique with a smearing parameter of 0.2 eV.[47] The lattice constant for Cu was calculated to be 3.64 Å using a Monkhosrst−Pack grid of (11 × 11 × 11), which is in good agreement with the experimental value 3.61 Å[48] and with previous calculations.[31,49,50] All of our calculations are spin-averaged except for those involving free molecular and atomic oxygen where the calculations are spin-polarized. We applied the climbing image nudged elastic bands (CI-NEB) method[51] to calculate the reaction barriers, where nine intermediate images are added in between the initial and final states. For the energetics of oxygen interstitials in Cu and NEB calculations, we used a supercell of 256 Cu atoms. We also carried out molecular dynamics (MD) simulation at 900 K for the diffusion of interstitial oxygen in the subsurface region and deep inside the Cu crystal. The surface effects are modeled with a 10-layer Cu(110) slab with 240 atoms.

3. RESULTS AND DISCUSSION

Our experiments include two steps starting with the first step of purposely introducing oxygen impurity into the Cu bulk by exposing the clean Cu(110) surface to O$_2$ flow, followed by subsequently switching to H$_2$ flow to reduce the Cu oxide as well as to deoxygenate O impurity in the Cu lattice. Figure 1 shows typical XPS spectra of the Cu 2p peaks obtained from the freshly cleaned Cu(110) surface (bottom panel) and its
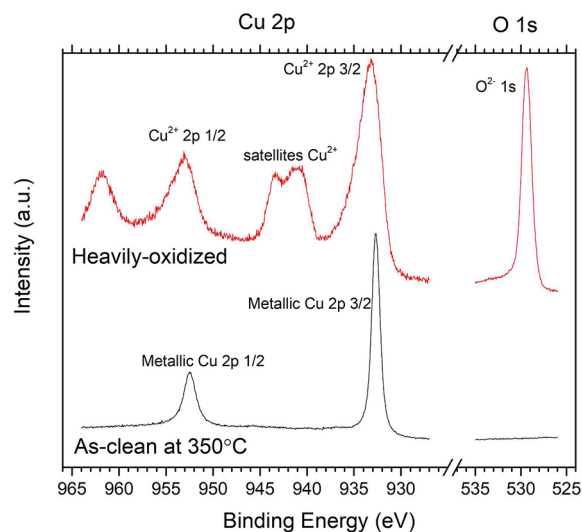
Figure 1. Photoelectron spectra of the Cu 2p and O 1s regions of the as-cleaned Cu(110) surface (black, lower panel) and its exposure to 1 Torr of oxygen gas for 1 h at 350 °C (red, upper panel).

subsequent exposure to pO_2 = 1 Torr for 60 min at T = 350 °C (upper panel). The as-cleaned surface remains the metallic state of Cu without any detectable intensity of the O 1s. Copper forms two thermodynamically stable oxides, CuO and Cu_2O, on reaction with oxygen, and the CuO formation spontaneously results in an inner Cu_2O layer. Such oxide layering can be understood from a thermodynamic equilibrium analysis and is also confirmed experimentally from cross-sectional electron microscopy images.[52−54] The XPS spectra of the oxidized surface display a Cu $2p3/2$ peak at the binding energy (BE) = 932.8 eV and the Cu $2p1/2$ peak at BE = 952.5 eV together with a series of strong shakeup satellites. These satellite structures are attributed to the spin−orbit splitting in the $2p^5 3d^9$ final states[55,56] and interpreted as the "fingerprint" of cupric ions.[57,58] Therefore, the Cu(110) was oxidized to form an outer CuO layer. This is further confirmed from the relatively symmetric O 1s spectra positioned at 529.5 eV, which can be primarily ascribed to the lattice oxygen in CuO.[57]

We then examine the reduction of the CuO layer by switching to a H_2 gas flow. To speed up the oxide reduction process, the sample temperature was raised to ∼520 °C in a H_2 pressure of 0.2 Torr. Figure 2 shows the evolution of the O 1s
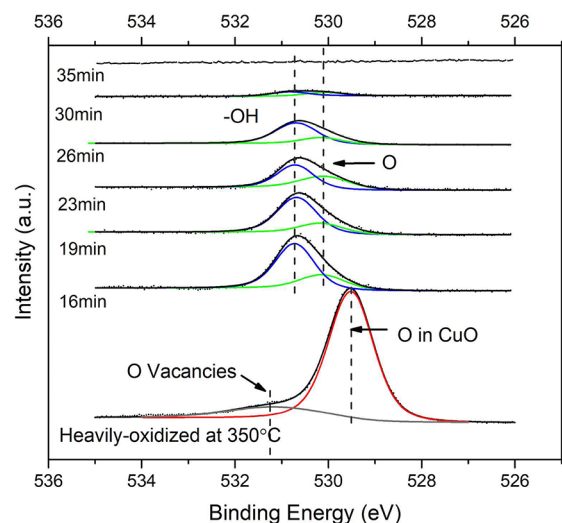
Figure 2. Temporal evolution of the photoemission spectra of the O 1s region for the exposure of the oxidized Cu(110) (red and at the bottom) to 0.2 Torr of H_2 gas flow at 520 °C. The O 1s spectrum (at the bottom) for the heavily oxidized Cu sample was taken at 350 °C in UHV. Red, green, and blue lines correspond to lattice O in CuO, and chemisorbed O and OH at the Cu(100) surface, respectively.

spectra under the presence of H_2 gas. The O 1s spectrum from the heavily oxidized surface is included in Figure 2 at the bottom as a reference, in which the major peak at 529.5 eV corresponds to lattice oxygen in CuO and the small shoulder around 531 eV can be attributed to the presence of oxygen vacancies in the CuO layer because the oxide was under UHV annealing (at 350 °C) and the oxide initially underwent some oxygen loss to form oxygen vacancies. The presence of oxygen vacancies in the CuO lattice shifts the electron state of adjacent atoms and may result in the shoulder, as shown in other studies.[59,60] The exposure of the oxidized surface to the H_2 gas flow leads to significant broadening of the O 1s spectra with the presence of a large shoulder at the higher binding energy side (see Figure S2 in the Supporting Information). After ∼16 min under H_2 gas, the entire O 1s shifts to a higher binding energy

and the peak corresponding to the lattice O in CuO disappears, indicating that the CuO layer has been reduced completely. The shifted O 1s spectra can be deconvoluted into two peaks positioned at 530.6 and 530.0 eV, which are ascribed to surface hydroxyl groups (OH)[61−66] and chemisorbed oxygen (O),[19,64] respectively. In our experiment, Cu $L_3M_{45}M_{45}$ Auger spectra were also taken since Cu 2p is not sufficient to confirm the chemical state of Cu. The Cu LMM Auger spectra confirmed that Cu is in the state of Cu^+ after prolonged vacuum annealing and Cu^o from the reduction with 0.1 Torr hydrogen (see Figure S3 in the Supporting Information). The combined O 1s and Cu LMM measurements allowed for discounting the presence of Cu_2O and the oxygen peak can be assigned to chemisorbed oxygen and OH. Because the O atom in hydroxyl groups has a shared electron with the H atom, oxygen is less negatively charged than chemisorbed O, O 1s peak for OH should be positioned at a higher binding energy than that of chemisorbed O.[67,68] As shown in Figure 2, the intensity of the OH and O peaks continues to shrink over time because of the gradual removal of these two species from the surface by their reactions with H atoms dissociated from adsorbed H_2 molecules to form H_2O molecules that desorb from the surface at the elevated temperature, that is, (i) H + O (chemisorbed) → OH, then (ii) OH + H → H_2O. This reaction sequence is further confirmed by the correlated evolution of the integrated intensity of the O and OH peaks shown later in Figure 4. Both the O and OH peaks disappear completely after ∼35 min in the presence of H_2 at 520 °C, indicating that the reactions have gone to completion and the Cu(110) surface becomes oxygen free.

We continue to monitor the Cu surface by continuously scanning the O 1s region while increasing the sample temperature in a stepwise fashion in the same H_2 gas pressure of 0.2 Torr. As indicated by the absence of any intensity of the O 1s spectra, the Cu surface remains oxygen free until reaching ∼580 °C. Figure 3 shows the evolution of the O 1s spectra at 580 °C and above in the continuous H_2 gas flow. As shown in Figure 3a, the Cu surface is first O-free, and the O 1s peak becomes visible after ∼3 min at 580 °C. The O 1s spectrum is initially symmetrical with the BE = 530.0 eV, which
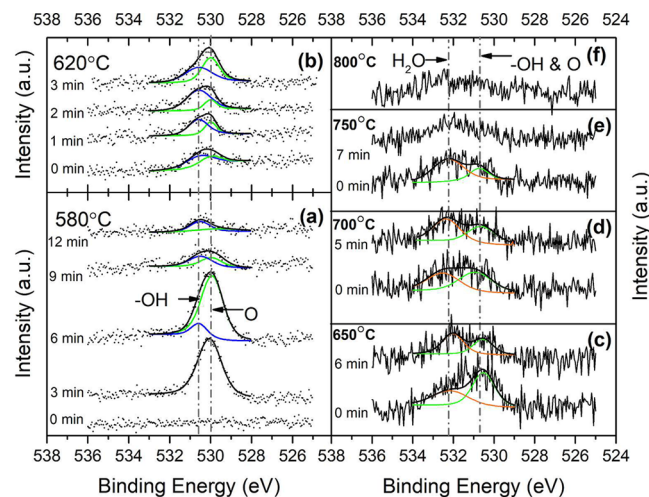
Figure 3. Temporal evolution of the O 1s spectra obtained from the fully reduced Cu(110) surface shown in Figure 2 and its subsequent stepwise temperature increase to 580 °C (a), 620 °C (b), 650 °C (c), 700 °C (d), 750 °C (e), and 800 °C (f) under 0.2 Torr of the constant flow of dry hydrogen.

corresponds to chemisorbed oxygen. The spectra become less symmetrical over time and a shoulder shows up at the higher binding energy, which corresponds to the formation of OH species because of the reaction of the chemisorbed oxygen with the H_2 gas, that is, $O + H \rightarrow OH$. By comparing with the 6 min spectrum, it can be seen that it took a few minutes for chemisorbed oxygen to react with adsorbed H to form a sufficient amount of OH detectable by XPS. The in situ XPS measurement shown here indicate that a critical temperature, ~580 °C, is required to drive appreciable outward diffusion of oxygen dissolved in the Cu bulk, which results in the surface segregation of oxygen atoms. As mentioned in the Experimental and Computational Methods, the Cu(110) crystal was initially treated by repeated cycles of ion sputtering and subsequent annealing at 600 °C to completely remove oxygen impurity in the Cu bulk via surface segregation. The absence of O 1s intensity from the surface of the annealed crystal (Figure 1) confirmed that there was no further surface segregation of oxygen from the bulk, indicating that the bulk was oxygen-free for the as-cleaned Cu crystal. Therefore, the oxygen impurity in the Cu bulk shown here was introduced in the oxidation step, as illustrated in Figure 1. It can be seen from Figure 3a that the overall intensity of the O 1s spectra grow stronger first with time (from 3 to 6 min), then turn over to shrink afterward, and become barely visible after 12 min. This trend in the O 1s intensity evolution indicates that the oxygen impurity in the bulk segregates to the surface, which results in the stronger intensity of the O 1s spectra. With the gradual depletion of the oxygen in the Cu lattice, the amount of the segregated O decreases and the continued removal of the oxygen from the surface by reacting with the H_2 gas results in the gradual diminishing of the overall intensity of the O 1s peak.

The sample temperature is then further increased to 620 °C in the same H_2 gas flow, and Figure 3b shows the time evolution of the O 1s spectra at this temperature. It can be seen that both the chemisorbed O and OH peaks become stronger again, indicating that there is additional surface segregation of oxygen atoms from the deeper region of bulk Cu to form chemisorbed O on the Cu surface, which subsequently reacts with adsorbed H to form OH species and then H_2O molecules that desorb from the surface. This trend for the surface segregation of O impurity from the even deeper region of bulk Cu can be further confirmed by the stepwise increasing of the sample temperature to 650 °C, 700 °C, 750 °C, and finally 800 °C, as shown in Figure 3c−f, respectively. As can be seen from Figure 3c−e, a peak at the binding energy of ~520 eV corresponding to H_2O became visible at the temperature above 650 °C. This further corroborates well with the proposed mechanism that H_2O forms at the surface by the reaction between segregated oxygen and adsorbed H. The peak at the lower binding energy can be ascribed to chemisorbed oxygen and OH species. Discrimination of chemisorbed O from OH species is difficult with the diminutive peak intensity. At 800 °C, the O 1s peak is barely visible and the prolonged holding at this temperature does not result in any further peak intensity in the O 1s region, indicating that the removal of oxygen impurity in the bulk Cu is complete.

Figure 4 shows further the temporal evolution of the intensity obtained from the integrated area under the O and OH peaks shown in Figure 3a, where the surface is initially both O and OH free when the sample temperature reaches 580 °C. The O peak shows up after ~1 min and reaches the maximum intensity after ~3 min. Thereafter, the OH peak starts to
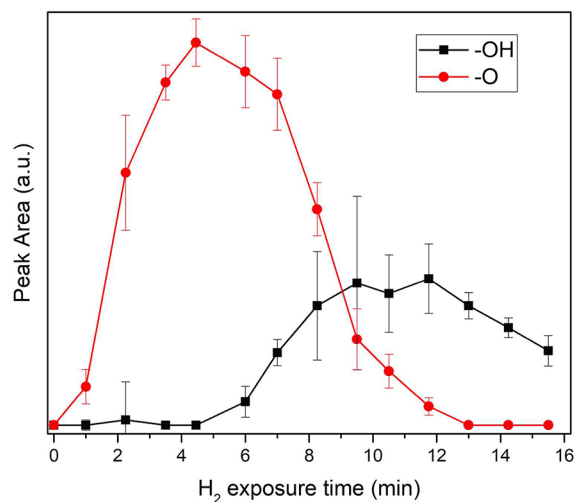
Figure 4. Time evolution of the integrated intensity of the O and OH peaks obtained from the Cu(110) surface during the deoxygenation process at 580 °C and 0.2 Torr of H_2 flow.

become visible, reaches the maximum intensity after ~9 min, and stays there for ~3 min, then gradually becomes weaker. Meanwhile, the intensity of the O peak drops significantly and down to nearly zero after 13 min. Such a correlated evolution in the O and OH peaks indicates that oxygen atoms in the bulk segregate to the surface and become chemisorbed O that then transforms to the OH state by reacting with H atoms dissociated from the adsorbed H_2 molecules. The subsequent recombination reaction of OH and H forms H_2O molecules that desorb from the surface. In this way, bulk dissolved oxygen is gradually depleted from the surface and subsurface region. It is worth mentioning that the deoxygenation of bulk dissolved oxygen cannot be observed with the high temperature alone (i.e., by annealing sample in UHV), as indicated from our AP-XPS measurements (see Figure S4 in the Supporting Information). This is because the segregated oxygen at the surface can exert strong repulsive force that hinders further segregation of oxygen from the bulk. The presence of H_2 gas is required for the deoxygenation because of the attractive interactions between adsorbed H and segregating oxygen as well as their recombination reactions to form H_2O molecules that desorb from the surface, as described above.

The relative distribution of O and OH species can be determined from the depth-profile analysis of the chemical state of oxygen. Figure 5 represents O 1s spectra obtained with various photon energies. The OH peak appears stronger at the smaller photon energies and the OH/O peak intensity ratio decreases from 0.297 to 0 as the photon energy increased from 650 to 1250 eV (the OH peak becomes barely visible at the photon energies of 1150 and 1250 eV). This indicates that the OH component is more surface sensitive than the O component, that is, OH species are located on the surface, while O species are present at the surface and subsurface region before they are completely depleted by reacting with hydrogen. It can be also noted from Figure 5 that a small peak located at BE = 532.3 eV is visible at the photon energies of 650 and 850 eV, which is ascribed to adsorbed H_2O molecules.[61] The absence of this peak at the photon energies of 1150 and 1250 eV indicates that H_2O molecules are located at the outer surface region, consistent with the proposed reaction of $OH + O \rightarrow H_2O$, where the formation of the OH species occurs at
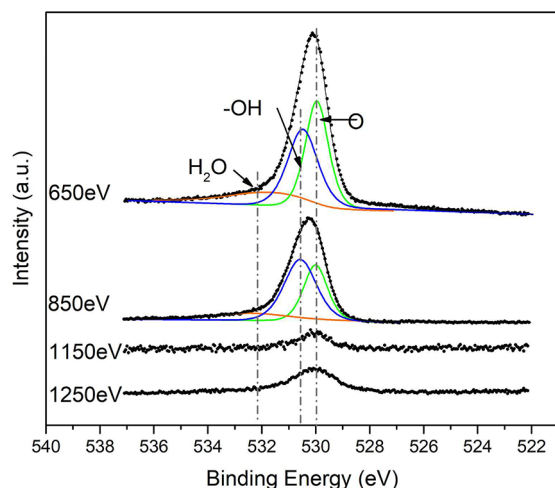
Figure 5. O 1s spectra measured at photon energies 650, 850, 1150, and 1250 eV, respectively, during the deoxygenation process at 620 °C and 0.2 Torr of H_2 flow.

the outer surface by the reaction between segregated O and hydrogen. The weak intensity of the H_2O peak indicates that the surface coverage of H_2O molecules is very low. This is due to the weak bonding between H_2O molecules and surface Cu atoms, for which the H_2O molecules formed from the reaction can easily desorb from the Cu surface.

To further investigate the deoxygenation process of bulk dissolved oxygen via its segregation to the surface and subsurface region, we employ DFT calculations to study the formation and migration energetics of interstitial oxygen in Cu lattice. In FCC (face-centered cubic) Cu lattice, there are two types of interstitial sites, that is, octahedral and tetrahedral sites (as shown schematically in Figure 6a) available for possible
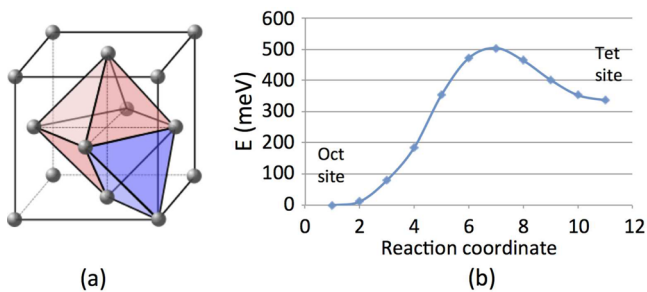
Figure 6. (a) Octahedral and tetrahedral sites for possible oxygen occupancy in FCC Cu lattice. (b) The minimum energy reaction path for oxygen migration from the octahedral site to the adjacent tetrahedral site. Reaction coordinates correspond to the initial site (octahedral site), nine intermediate sites, and the final site (tetrahedral site), respectively.

oxygen occupancy. We first compare the relative stability of oxygen adsorbed at these two types of the interstitial sites. Our DFT results indicate that oxygen atoms prefer the octahedral sites and are 0.32 eV more stable than at the tetrahedral sites. It is also found from our DFT computations that it is energetically more favorable to split an oxygen molecule into two oxygen atoms that occupy the octahedral sites, which results in an energy gain by 0.22 eV/atom or 0.45 eV per O_2 molecule.

We then examine the energy barriers for the migration of interstitial oxygen atoms. As shown in Figure 6a, the segregation of bulk-dissolved oxygen to the surface region

requires the sequential migration of an oxygen atom from an octahedral site to its adjacent tetrahedral site and then to another octahedral site. We then perform NEB calculations to quantitatively study the transition from the octahedral site to the tetrahedral site. The diffusion potential energy along the reaction path is given in Figure 6b, which shows an activation barrier of about 0.5 eV for the migration of oxygen atoms through the interstitial sites. The value of our calculated diffusion barrier for oxygen migration is in reasonable agreement with experiments,[69] corroborating well with the interstitial diffusion mechanism for the segregation of bulk dissolved oxygen. Meanwhile, we have also performed MD simulations to examine the diffusion of interstitial oxygen atoms in bulk Cu crystal and oxygen atoms in the near surface region. Figure 7 shows the mean squared displacements (MSD)
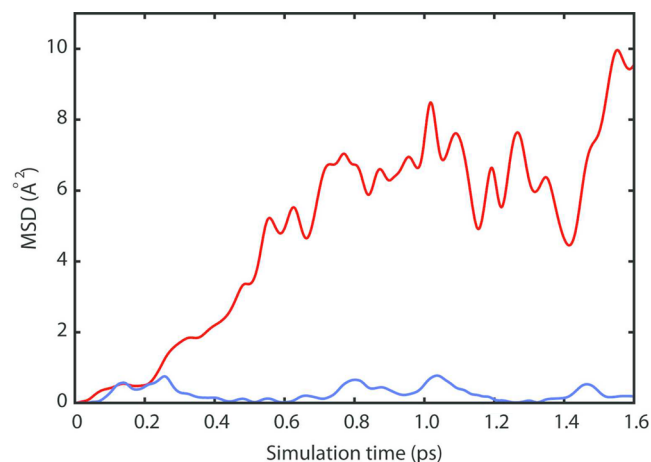
Figure 7. MSD curves vs time from the MD simulations of the diffusion of oxygen atoms at 627 °C, where the red and blue lines correspond to the oxygen atoms in bulk and close to the surface, respectively.

measured from our MD simulations of the diffusion of oxygen atoms at 900 K (627 °C). For the oxygen atom in bulk (blue curve in Figure 7), we observe a very slow diffusion rate (actually, no diffusion within the simulation time), which is consistent with the calculated larger diffusion barrier of about 0.5 eV. For the oxygen atom close to the (110) surface, we observe relatively rapid diffusion of the oxygen atom toward the surface (red curve in Figure 7), indicating that the presence of a surface facilitates the oxygen surface segregation. Once these oxygen atoms reach the surface, they can presumably react with adsorbed hydrogen.

4. CONCLUSIONS

Using AP-XPS, we have demonstrated that the oxidation of Cu(110) under the ambient pressure conditions results in bulk dissolved oxygen in Cu and the segregation of bulk dissolved oxygen to the surface and subsurface region can be tuned by the flow of H_2 gas at elevated temperature. Our in situ AP-XPS measurements showed that a critical temperature of ∼580 °C is required for driving surface segregation of bulk-dissolved oxygen and this deoxygenation process is tunable with stepwise increase of temperature to drive the oxygen segregation to the surface and subsurface regions from deeper in the bulk of Cu. We envisage that the approach demonstrated in this work, monitoring the deoxygenation process by following evolution of the integrated intensity of the O 1s spectra as a function of

time and temperature, can be employed to quantify the total amount of oxygen dissolved in the bulk by simultaneously acquiring Cu 2p spectra at a different photo energy that would provide the same level of detection depth for spectra baseline for both elements. Because the chemical reactivity of surface oxygen can differ dramatically from bulk-dissolved oxygen, surface oxygen has been invoked to explain modified adsorption behaviors of metal surfaces. On top of that, controlling the segregation-induced enrichment of oxygen in the surface region, as demonstrated by our results, is a potentially useful strategy for optimizing the activity and stability of metal surfaces.

■ ASSOCIATED CONTENT

ⓢ Supporting Information

The Supporting Information is available free of charge on the ACS Publications website at DOI: 10.1021/acs.jpcc.7b12030.

SI-1: Carbon-free Cu(110) crystal; SI-2: XPS curve fitting parameters; SI-3: Reduction of the oxidized Cu(110) at 350 °C and 0.1 Torr of H_2 gas flow; SI-4: Cu $L_3M_{45}M_{45}M_{45}$ spectra; SI-5: O 1s for oxide reduction induced by vacuum annealing (PDF).

■ AUTHOR INFORMATION

Corresponding Author
*E-mail: gzhou@binghamton.edu.

ORCID ⓞ
Guangwen Zhou: 0000-0002-9243-293X

Notes
The authors declare no competing financial interest.

■ REFERENCES

(1) Eren, B.; Heine, C.; Bluhm, H.; Somorjai, G. A.; Salmeron, M. Catalyst Chemical State during CO Oxidation Reaction on Cu(111) Studied with Ambient-Pressure X-Ray Photoelectron Spectroscopy and Near Edge X-Ray Adsorption Fine Structure Spectroscopy. *J. Am. Chem. Soc.* **2015**, *137* (34), 11186−11190.

(2) Wrobel, R. J.; Becker, S.; Weiss, H. Influence of Subsurface Oxygen in the Catalytic CO Oxidation on Pd(111). *J. Phys. Chem. C* **2015**, *119* (10), 5386−5394.

(3) Setvin, M.; Aschauer, U.; Scheiber, P.; Li, Y.-F.; Hou, W.; Schmid, M.; Selloni, A.; Diebold, U. Reaction of O2 with Subsurface Oxygen Vacancies on TiO2 Anatase (101). *Science (Washington, DC, U. S.)* **2013**, *341* (6149), 988−991.

(4) Search, H.; Journals, C.; Contact, A.; Iopscience, M.; Simul, M.; Address, I. P.; Mendelev, M. I.; Srolovitz, D. J. Impurity Effects on Grain Boundary Migration. *Model. Simul. Mater. Sci. Eng.* **2002**, *10* (6), R79−R109.

(5) Tang, F.; Gianola, D. S.; Moody, M. P.; Hemker, K. J.; Cairney, J. M. Observations of Grain Boundary Impurities in Nanocrystalline Al and Their Influence on Microstructural Stability and Mechanical Behaviour. *Acta Mater.* **2012**, *60*, 1038−1047.

(6) Trinkaus, H.; Singh, B. N.; Foreman, A. J. E. Mechanisms for Decoration of Dislocations by Small Dislocation Loops under Cascade Damage Conditions. *J. Nucl. Mater.* **1997**, *249*, 91−102.

(7) Trinkaus, H.; Singh, B. N.; Foreman, A. J. E. Segregation of Cascade Induced Interstitial Loops at Dislocations: Possible Effect on Initiation of Plastic Deformation. *J. Nucl. Mater.* **1997**, *251* (0), 172−187.

(8) Jiang, Y.; Smith, J. R.; Evans, A. G. First Principles Assessment of Metal/oxide Interface Adhesion. *Appl. Phys. Lett.* **2008**, *92* (14), 1−4.

(9) Ghazisaeidi, M.; Trinkle, D. R. Interaction of Oxygen Interstitials with Lattice Faults in Ti. *Acta Mater.* **2014**, *76*, 82−86.

(10) Sakuraya, S.; Takahashi, K.; Wang, S.; Hashimoto, N.; Ohnuki, S. Physical Properties of α-Fe upon the Introduction of H, He, C, and N. *Solid State Commun.* **2014**, *195*, 70−73.

(11) Choi, C. H.; Lim, H. K.; Chung, M. W.; Park, J. C.; Shin, H.; Kim, H.; Woo, S. I. Long-Range Electron Transfer over Graphene-Based Catalyst for High-Performing Oxygen Reduction Reactions: Importance of Size, N-Doping, and Metallic Impurities. *J. Am. Chem. Soc.* **2014**, *136* (25), 9070−9077.

(12) Starr, D. E.; Liu, Z.; Hävecker, M.; Knop-Gericke, A.; Bluhm, H. Investigation of Solid/vapor Interfaces Using Ambient Pressure X-Ray Photoelectron Spectroscopy. *Chem. Soc. Rev.* **2013**, *42* (13), 5833−5857.

(13) Shavorskiy, A.; Müller, K.; Newberg, J. T.; Starr, D. E.; Bluhm, H. Hydroxylation of Ultrathin Al 2 O 3 /NiAl(110) Films at Environmental Humidity. *J. Phys. Chem. C* **2014**, *118* (50), 29340−29349.

(14) Frank Ogletree, D.; Bluhm, H.; Hebenstreit, E. D.; Salmeron, M. Photoelectron Spectroscopy under Ambient Pressure and Temperature Conditions. *Nucl. Instrum. Methods Phys. Res., Sect. A* **2009**, *601*, 151−160.

(15) Salmeron, M.; Schlögl, R. Ambient Pressure Photoelectron Spectroscopy: A New Tool for Surface Science and Nanotechnology. *Surf. Sci. Rep.* **2008**, *63*, 169.

(16) Li, J.; Zhou, G. Density Functional Theory Study of O-H and C-H Bond Scission of Methanol Catalyzed by a Chemisorbed Oxygen Layer on Cu(111). *Surf. Sci.* **2016**, *646*, 288−297.

(17) Breen, J. P.; Ross, J. R. H. Methanol Reforming for Fuel-Cell Applications: Development of Zirconia-Containing Cu−Zn−Al Catalysts. *Catal. Today* **1999**, *51*, 521−533.

(18) Sakong, S.; Groß, A. Density Functional Theory Study of the Partial Oxidation of Methanol on Copper Surfaces. *J. Catal.* **2005**, *231*, 420−429.

(19) Bluhm, H.; Hävecker, M.; Knop-Gericke, A.; Kleimenov, E.; Schlögl, R.; Teschner, D.; Bukhtiyarov, V. I.; Ogletree, D. F.; Salmeron, M. Methanol Oxidation on a Copper Catalyst Investigated Using in Situ X-Ray Photoelectron Spectroscopy. *J. Phys. Chem. B* **2004**, *108*, 14340−14347.

(20) Gokhale, A. A.; Dumesic, J. A.; Mavrikakis, M. Article On the Mechanism of Low-Temperature Water Gas Shift Reaction on Copper On the Mechanism of Low-Temperature Water Gas Shift Reaction on Copper. *J. Am. Chem. Soc.* **2008**, *130* (33), 1402−1414.

(21) Chinchen, G. C.; Spencer, M. S.; Waugh, K. C.; Whan, D. A. Promotion of Methanol Synthesis and the Water-Gas Shift Reactions by Adsorbed Oxygen on Supported Copper Catalysts. *J. Chem. Soc., Faraday Trans. 1* **1987**, *83* (7), 2193−2212.

(22) Wang, X.; Rodriguez, J. A.; Hanson, J. C.; Gamarra, D.; Martínez-Arias, A.; Fernández-García, M. In Situ Studies of the Active Sites for the Water Gas Shift Reaction over Cu−CeO 2 Catalysts: Complex Interaction between Metallic Copper and Oxygen Vacancies of Ceria. *J. Phys. Chem. B* **2006**, *110* (1), 428−434.

(23) Goli, P.; Ning, H.; Li, X.; Lu, C. Y.; Novoselov, K. S.; Balandin, A. A. Thermal Properties of Graphene-Copper-Graphene Heterogeneous Films. *Nano Lett.* **2014**, *14* (3), 1497−1503.

(24) Hwang, J.; Yoon, T.; Jin, S. H.; Lee, J.; Kim, T. S.; Hong, S. H.; Jeon, S. Enhanced Mechanical Properties of Graphene/copper Nanocomposites Using a Molecular-Level Mixing Process. *Adv. Mater.* **2013**, *25*, 6724−6729.

(25) Tay, R. Y.; Griep, M. H.; Mallick, G.; Tsang, S. H.; Singh, R. S.; Tumlin, T.; Teo, E. H. T.; Karna, S. P. Growth of Large Single-Crystalline Two-Dimensional Boron Nitride Hexagons on Electropolished Copper. *Nano Lett.* **2014**, *14* (2), 839−846.

(26) Favaro, M.; Xiao, H.; Cheng, T.; Goddard, W. A.; Yano, J.; Crumlin, E. J. Subsurface Oxide Plays a Critical Role in CO₂ Activation by Cu(111) Surfaces to Form Chemisorbed CO₂, the First Step in Reduction of C 2. *Proc. Natl. Acad. Sci. U. S. A.* **2017**, *114*, 6706−6711.

(27) Hao, Y.; Bharathi, M. S.; Wang, L.; Liu, Y.; Chen, H.; Nie, S.; Wang, X.; Chou, H.; Tan, C.; Fallahazad, B.; et al. The Role of Surface Oxygen in the Growth of Large Single-Crystal Graphene on Copper. *Science* **2013**, *342* (6159), 720−723.

(28) Blume, R.; Kidambi, P. R.; Bayer, B. C.; Weatherup, R. S.; Wang, Z.-J.; Weinberg, G.; Willinger, M.-G.; Greiner, M.; Hofmann, S.; Knop-Gericke, A.; Schlögl, R. The Influence of Intercalated Oxygen on the Properties of Graphene on Polycrystalline Cu under Various Environmental Conditions. *Phys. Chem. Chem. Phys.* **2014**, *16* (47), 25989−26003.

(29) Braeuninger-Weimer, P.; Brennan, B.; Pollard, A. J.; Hofmann, S. Understanding and Controlling Cu-Catalyzed Graphene Nucleation: The Role of Impurities, Roughness, and Oxygen Scavenging. *Chem. Mater.* **2016**, *28* (24), 8905−8915.

(30) Rodriguez, J. A.; Kim, J. Y.; Hanson, J. C.; Pérez, M.; Frenkel, A. I. Reduction of CuO in H₂: In Situ Time-Resolved XRD Studies. *Catal. Lett.* **2003**, *85*, 247−254.

(31) Li, L.; Mi, X.; Shi, Y.; Zhou, G. Precursor to the Onset of the Bulk Oxidation of Cu(100). *Phys. Rev. Lett.* **2012**, *108*, 176101.

(32) Kim, J. Y.; Hanson, J. C.; Frenkel, A. I.; Lee, P. L.; Rodriguez, J. a. Reaction of CuO with Hydrogen Studied by Using Synchrotron-Based X-Ray Diffraction. *J. Phys.: Condens. Matter* **2004**, *16*, S3479−S3484.

(33) Wang, X.; Hanson, J. C.; Frenkel, A. I.; Kim, J. Y.; Rodriguez, J. A. Time-Resolved Studies for the Mechanism of Reduction of Copper Oxides with Carbon Monoxide: Complex Behavior of Lattice Oxygen and the Formation of Suboxides. *J. Phys. Chem. B* **2004**, *108*, 13667−13673.

(34) Kim, J. Y.; Rodriguez, J. A.; Hanson, J. C.; Frenkel, A. I.; Lee, P. L. Reduction of CuO and Cu₂O with H2: H Embedding and Kinetic Effects in the Formation of Suboxides. *J. Am. Chem. Soc.* **2003**, *125*, 10684−10692.

(35) Yuan, L.; Yin, Q.; Wang, Y.; Zhou, G. CuO Reduction Induced Formation of CuO/Cu₂O Hybrid Oxides. *Chem. Phys. Lett.* **2013**, *590*, 92−96.

(36) Li, L.; Luo, L.; Ciston, J.; Saidi, W. A.; Stach, E. A.; Yang, J. C.; Zhou, G. Surface-Step-Induced Oscillatory Oxide Growth. *Phys. Rev. Lett.* **2014**, *113*, 136104.

(37) Zhou, G.; Luo, L.; Li, L.; Ciston, J.; Stach, E. A.; Yang, J. C. Step-Edge-Induced Oxide Growth during the Oxidation of Cu Surfaces. *Phys. Rev. Lett.* **2012**, *109*, 235502.

(38) Reitz, J. B.; Solomon, E. I. Propylene Oxidation on Copper Oxide Surfaces: Electronic and Geometric Contributions to Reactivity and Selectivity. *J. Am. Chem. Soc.* **1998**, *120* (44), 11467−11478.

(39) Hatcher, L. Q.; Karlin, K. D. Oxidant Types in Copper-Dioxygen Chemistry: The Ligand Coordination Defines the Cu(n)-O₂ Structure and Subsequent Reactivity. *JBIC, J. Biol. Inorg. Chem.* **2004**, *9*, 669−683.

(40) Kresse, G.; Hafner, J. Ab Initio Molecular Dynamics for Liquid Metals. *Phys. Rev. B: Condens. Matter Mater. Phys.* **1993**, *47*, 558−561.

(41) Kresse, G.; Hafner, J. Ab Initio Molecular-Dynamics Simulation of the Liquid-Metal-Amorphous-Semiconductor Transition in Germanium. *Phys. Rev. B: Condens. Matter Mater. Phys.* **1994**, *49*, 14251−14269.

(42) Kresse, G.; Furthmüller, J. Efficiency of Ab-Initio Total Energy Calculations for Metals and Semiconductors Using a Plane-Wave Basis Set. *Comput. Mater. Sci.* **1996**, *6*, 15−50.

(43) Kresse, G.; Furthmüller, J. Efficient Iterative Schemes for Ab Initio Total-Energy Calculations Using a Plane-Wave Basis Set. *Phys. Rev. B: Condens. Matter Mater. Phys.* **1996**, *54*, 11169−11186.

(44) Perdew, J.; Chevary, J.; Vosko, S.; Jackson, K.; Pederson, M.; Singh, D.; Fiolhais, C. Atoms, Molecules, Solids, and Surfaces: Applications of the Generalized Gradient Approximation for Exchange and Correlation. *Phys. Rev. B: Condens. Matter Mater. Phys.* **1992**, *46*, 6671−6687.

(45) Kresse, G.; Joubert, D. From Ultrasoft Pseudopotentials to the Projector Augmented-Wave Method. *Phys. Rev. B: Condens. Matter Mater. Phys.* **1999**, *59*, 1758−1775.

(46) Blöchl, P. E. Projector Augmented-Wave Method. *Phys. Rev. B: Condens. Matter Mater. Phys.* **1994**, *50*, 17953−17979.

(47) Monkhorst, H. J.; Pack, J. D. Special Points for Brillouin-Zone Integrations. *Phys. Rev. B* **1976**, *13*, 5188−5192.

(48) Ashcroft, N. W.; Mermin, N. D. *Solid State Physics*; Saunders College, 1976.

(49) Li, L.; Liu, Q.; Li, J.; Saidi, W. A.; Zhou, G. Kinetic Barriers of the Phase Transition in the Oxygen Chemisorbed Cu(110)-(2 × 1)-O as a Function of Oxygen Coverage. *J. Phys. Chem. C* **2014**, *118*, 20858−20866.

(50) Liem, S.; Kresse, G.; Clarke, J. H. R. First Principles Calculation of Oxygen Adsorption and Reconstruction of Cu(110) Surface. *Surf. Sci.* **1998**, *415*, 194−211.

(51) Henkelman, G.; Uberuaga, B. P.; Jónsson, H. Climbing Image Nudged Elastic Band Method for Finding Saddle Points and Minimum Energy Paths. *J. Chem. Phys.* **2000**, *113*, 9901−9904.

(52) Yuan, L.; Zhou, G. Enhanced CuO Nanowire Formation by Thermal Oxidation of Roughened Copper. *J. Electrochem. Soc.* **2012**, *159*, C205−C209.

(53) Mema, R.; Yuan, L.; Du, Q.; Wang, Y.; Zhou, G. Effect of Surface Stresses on CuO Nanowire Growth in the Thermal Oxidation of Copper. *Chem. Phys. Lett.* **2011**, *512*, 87−91.

(54) Yuan, L.; Wang, Y.; Mema, R.; Zhou, G. Driving Force and Growth Mechanism for Spontaneous Oxide Nanowire Formation during the Thermal Oxidation of Metals. *Acta Mater.* **2011**, *59*, 2491−2500.

(55) Ghijsen, J.; Tjeng, L.; van Elp, J.; Eskes, H.; Westerink, J.; Sawatzky, G.; Czyzyk, M. Electronic Structure of Cu2O and CuO. *Phys. Rev. B: Condens. Matter Mater. Phys.* **1988**, *38*, 11322−11330.

(56) Kim, K. S. Charge Transfer Transition Accompanying X-Ray Photoionization in Transition-Metal Compounds. *J. Electron Spectrosc. Relat. Phenom.* **1974**, *3*, 217−226.

(57) Robert, T.; Bartel, M.; Offergeld, G. Characterization of Oxygen Species Adsorbed on Copper and Nickel Oxides by X-Ray Photoelectron Spectroscopy. *Surf. Sci.* **1972**, *33*, 123−130.

(58) Robert, T.; Offergeld, G. Pectres de Photoélectrons X de Composés Solides de Cuivre Relation Entre La Présence de Raies Satellites et L'état D'oxydation Du Cuivre. *Phys. status solidi* **1972**, *14*, 277−282.

(59) Hardacre, C.; Roe, G. M.; Lambert, R. M. Structure, Composition and Thermal Properties of Cerium Oxide Films on Platinum {111}. *Surf. Sci.* **1995**, *326*, 1−10.

(60) Wang, Y.; Lu, Y.; Zhan, W.; Xie, Z.; Kuang, Q.; Zheng, L. Synthesis of Porous Cu₂O/CuO Cages Using Cu-Based Metal-Organic Frameworks as Templates and Their Gas-Sensing Properties. *J. Mater. Chem. A* **2015**, *3*, 12796−12803.

(61) Andersson, K.; Ketteler, G.; Bluhm, H.; Yamamoto, S.; Ogasawara, H.; Pettersson, L. G. M.; Salmeron, M.; Nilsson, A. Bridging the Pressure Gap in Water and Hydroxyl Chemistry on Metal Surfaces: The Cu(110) Case. *J. Phys. Chem. C* **2007**, *111*, 14493−14499.

(62) Biesinger, M. C.; Lau, L. W. M.; Gerson, A. R.; Smart, R. S. C. Resolving Surface Chemical States in XPS Analysis of First Row Transition Metals, Oxides and Hydroxides: Sc, Ti, V, Cu and Zn. *Appl. Surf. Sci.* **2010**, *257* (3), 887−898.

(63) Andersson, K.; Gómez, A.; Glover, C.; Nordlund, D.; Öström, H.; Schiros, T.; Takahashi, O.; Ogasawara, H.; Pettersson, L. G. M.; Nilsson, A. Molecularly Intact and Dissociative Adsorption of Water on Clean Cu(110): A Comparison with the water/Ru(001) System. *Surf. Sci.* **2005**, *585*, L183−L189.

(64) Yamamoto, S.; Andersson, K.; Bluhm, H.; Ketteler, G.; Starr, D. E.; Schiros, T.; Ogasawara, H.; Pettersson, L. G. M.; Salmeron, M.; Nilsson, A. Hydroxyl-Induced Wetting of Metals by Water at near-Ambient Conditions. *J. Phys. Chem. C* **2007**, *111* (22), 7848−7850.

(65) Deng, X.; Herranz, T.; Weis, C.; Bluhm, H.; Salmeron, M. Adsorption of Water on Cu_2O and Al_2O_3 Thin Films. *J. Phys. Chem. C* **2008**, *112*, 9668−9672.

(66) Andersson, K.; Ketteler, G.; Bluhm, H.; Yamamoto, S.; Ogasawara, H.; Pettersson, L. G. M.; Salmeron, M.; Nilsson, A. Autocatalytic Water Dissociation on Cu(110) at near Ambient Conditions. *J. Am. Chem. Soc.* **2008**, *130* (9), 2793−2797.

(67) Michaelides, A.; Alavi, A.; King, D. A. Insight into H2O-Ice Adsorption and Dissociation on Metal Surfaces from First-Principles Simulations. *Phys. Rev. B: Condens. Matter Mater. Phys.* **2004**, *69*, 113404.

(68) Meng, S.; Wang, E. G.; Gao, S. Water Adsorption on Metal Surfaces: A General Picture from Density Functional Theory Studies. *Phys. Rev. B: Condens. Matter Mater. Phys.* **2004**, *69*, 195404.

(69) Narula, M. L.; Tare, V. B.; Worrell, W. L. Diffusivity and Solubility of Oxygen in Solid Copper Using Potentiostatic and Potentiometric Techniques. *Metall. Trans. B* **1983**, *14*, 673−677.